

Polymerization-Induced Emission (PIE) of Multifunctional Polyamides Synthesized by Ugi Polymerization and Targeted Imaging for Lysosomes

Xue Meng^a, Tingting Hao, Da Zhang^a, Ronghui Zhao^{a,b}, Hongmei Liu^a, Pengfei Zhang^a,

Kuilin Deng^{a*}

^aCollege of Chemistry and Materials Science, Hebei University, Baoding 071002,
China; ^b Department of Clinical Pharmacy, Affiliated Hospital of Hebei University,
Baoding 071002, China

*Corresponding author: Email: dengkl_hbu@163.com

Chemicals and Reagents:.....	2
Instruments and Measurements:	2
Synthesis of small molecule model compounds (AM).....	3
Table S1. Different structures of synthesized PAMs.	3
Table S2. Yield, M_n , PDI and quantum yield of PAMs.	4
Fig. S1. ¹ H NMR spectra of PAMs	5
Fig. S2. FT-IR spectra of PAMs.....	6
Fig. S3. GPC curves of PAMs.....	7
Fig. S4. UV and Fluorescence Spectra of PAMs and AM.	8
Fig. S5. M_n change of PAM-TB with polymerization time.....	8
Fig. S6. Fluorescence spectra of PAM-TB solution with different concentration.	9
Fig. S7. Particle size plots of PAM-TB at different concentrations.....	9
Fig. S8. The effect of anions on fluorescence intensity.	9
Fig. S9. Schematic illustration of PAMs reuse.....	10
Fig. S10. Visual test paper for Fe ³⁺ ions	11
Fig. S11. Cell imaging experiments of PAM-TB.....	11
Fig. S12. Colocalization Coefficient of PAM-TM and LysoTracker Red in PC-12 cell.	12

Fig. S13. Colocalization Coefficient of PAM-TM and LysoTracker Red in HeLa cell.	12
Fig. S14. Photobleaching resistance map of PAM-TM in cells.	13
Fig. S15. Effects of PAM-TM on PC-12 cell viability.....	13
Fig. S16. Fluorescence intensity of PAM-TM in the presence or absence of interfering ions.....	14
Table S3. A comparison between PAM-TM probes and the reported Fe ³⁺ -responsive fluorescent probes.....	15

Chemicals and Reagents:

Oxalic acid , succinic acid and adipic acid were purchased from Tianjin Kemiou Chemical Reagent Co., Ltd. Glutaraldehyde, terephthalaldehyde and 2-Morpholinoethyl isocyanide were provided by Aladdin Company (Shanghai, China). Benzaldehyde, propanoic acid, *t*-butylisonitrile and *N*-(2-aminoethyl)-morpholine were purchased from Shanghai McLean Biochemical Co., Ltd. (China). Unless otherwise stated, all chemicals and reagents were obtained from commercial suppliers and used as received without further purification. PC-12 cells were purchased from Procell Biotechnology and thiazole blue tetrazole ammonium bromide (MTT) from Solarbio Life Sciences.

Instruments and Measurements:

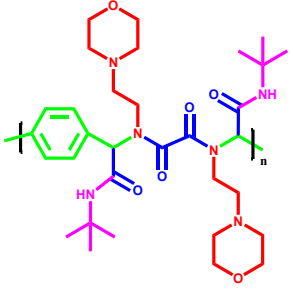
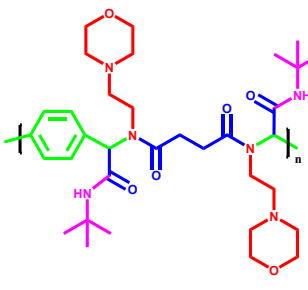
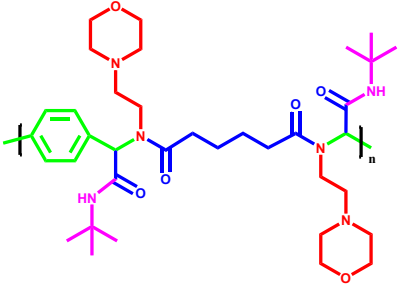
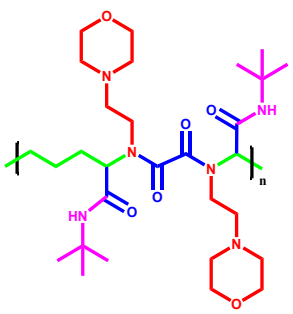
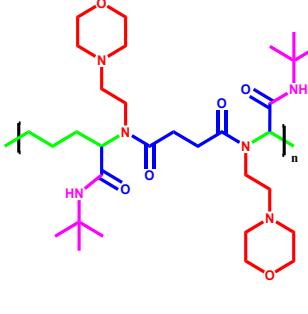
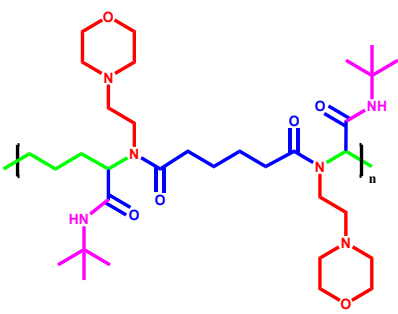
In the experiments, we scanned Fourier transform infrared spectra (FT-IR) of PAMs in the wavenumber range of 400-4000 cm⁻¹ using a Bruker Tensor 27 FT-IR spectrometer with a Specac Quest ATR accessory. ¹H NMRs (400 MHz) of PAMs were recorded on a Bruker AVANCE III spectrometer at room temperature with tetramethylsilane (TMS) as an internal standard. The molecular weight (M_n) and polydispersity index (PDI) of prepared PAMs were determined using a gel

permeation chromatography (GPC) system (Agilent 1200). *N, N*-dimethylformamide (DMF) with 0.1% lithium bromide as the elution solvent and polystyrene as the molecular weight standard. The average size of aggregated particles in solution was measured by dynamic light scattering (DLS) Zetasizer nano-ZSE. MTT analyses were conducted on a microplate reader (TECAN infinite M1000 Pro). Confocal fluorescence images were performed on inverted Zeiss LSM800.

Synthesis of small molecule model compounds (AM)

According to the synthesis steps for PAMs, *N*-(2-Aminoethyl)-morpholine (3 mmol, 0.40 g) and benzaldehyde (3 mmol, 0.32 g) were dissolved in 6 mL DMSO and reacted for 1 h to produce imine intermediates. Then, propionic acid (3 mmol, 0.23 g) and *t*-butylisocyanide (3.5 mmol, 0.30 g) were added to the reaction system, and the reaction was completed over 24 h. The crude product was purified by a column chromatography with an eluent of ethyl acetate and ethanol (10:1, v/v) mixture. The pure small molecule model compound, *N*-(2-*tert*-butylamino)-2-carbonyl-1-phenylethyl)-*N*-(2-morpholine ethyl) propionamide, abbreviated as AM, was obtained as yellow solid with a yield of 88%.

Table S1. Different structures of synthesized PAMs.

PAM-TO	PAM-TB	PAM-TA
		
PAM-GO	PAM-GB	PAM-GA
		
PAM-TM		

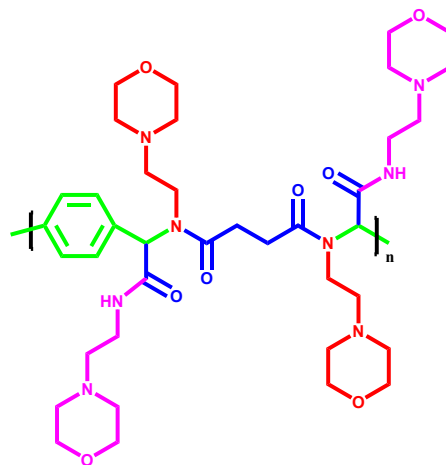


Table S2. Yield, M_n , PDI and quantum yield of PAMs.

Sample	Yield (%)	$M_n \times 10^4$ g/mol	PDI	Quantum yield (%)
PAM-TO	75.36	1.10	1.79	26.8
PAM-TB	78.96	1.60	1.66	23.4
PAM-TA	77.68	2.20	1.75	19.6
PAM-GO	68.52	0.71	1.72	12.1
PAM-GB	66.75	0.83	1.84	10.8
PAM-GA	70.25	0.88	1.91	8.60
PAM-TM	62.13	1.40	1.47	14.3

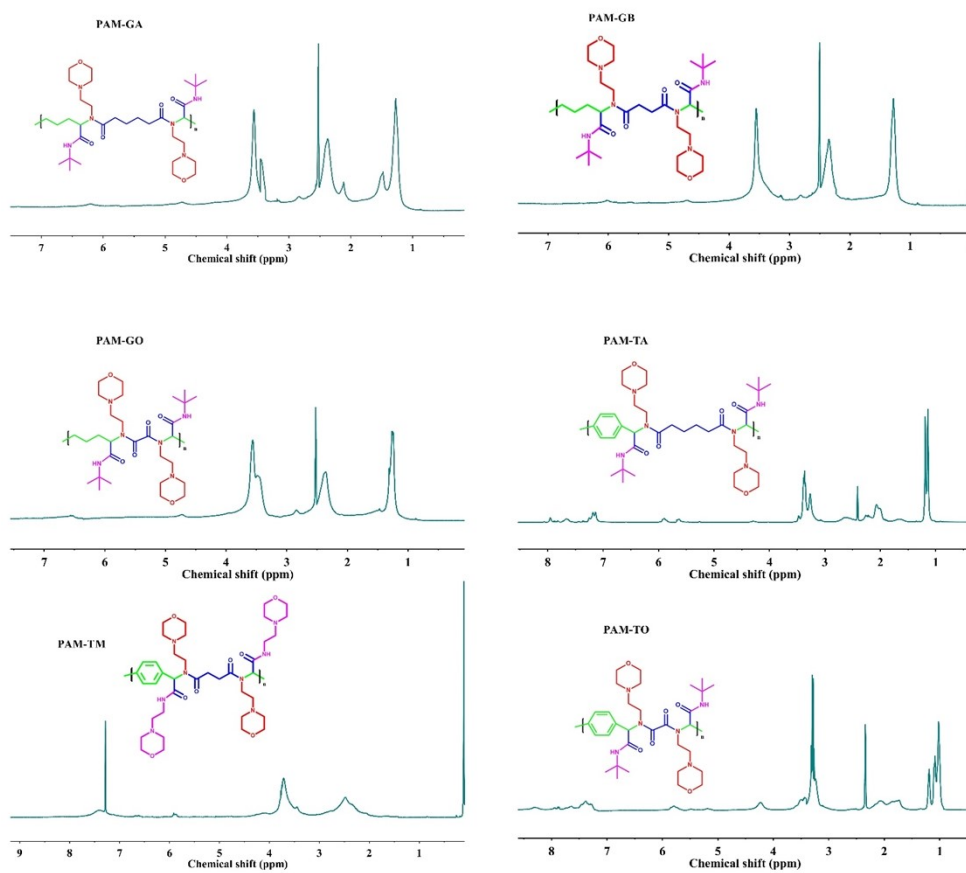


Fig. S1. 1H NMR spectra of PAMs

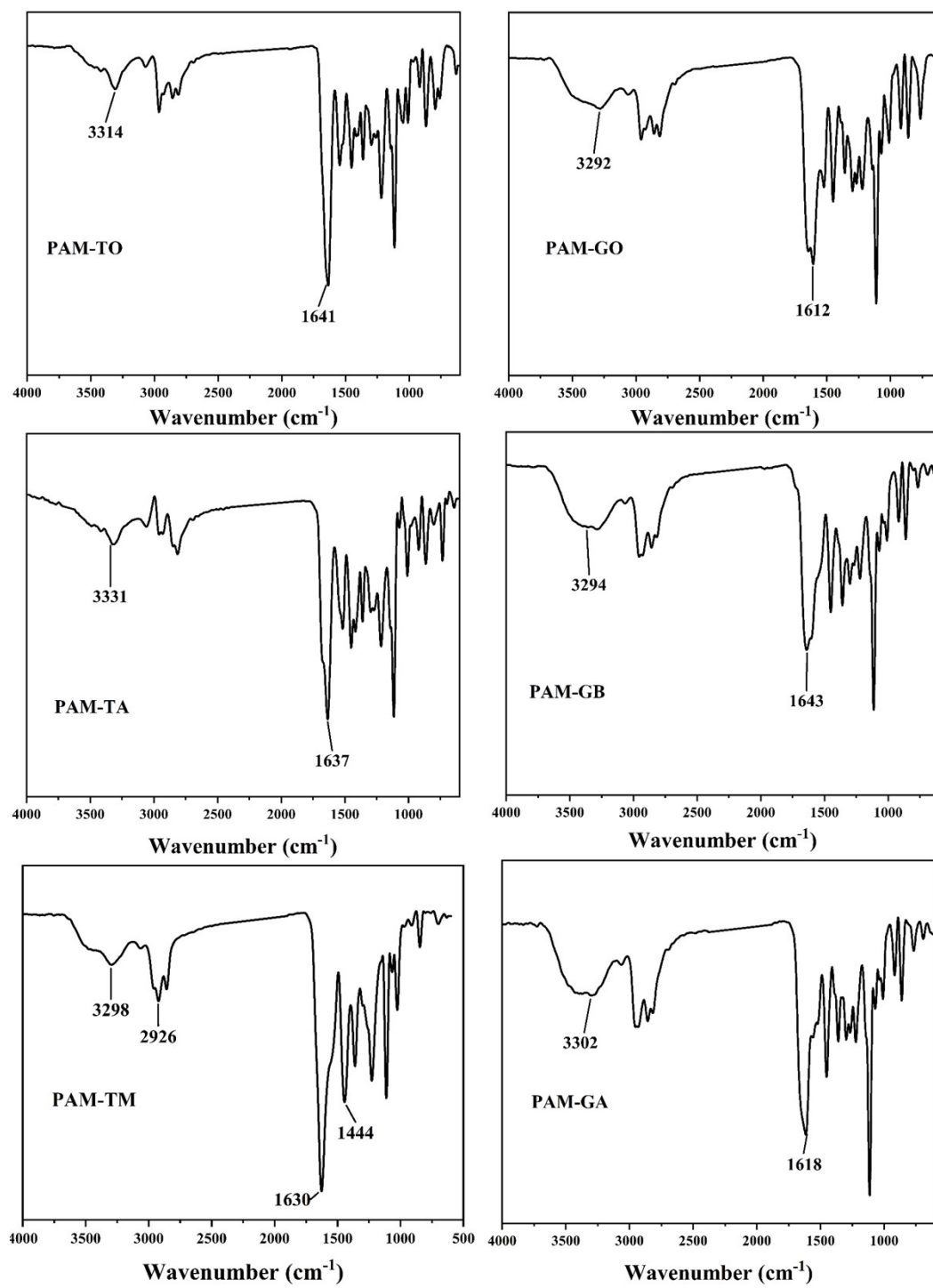


Fig. S2. FT-IR spectra of PAMs

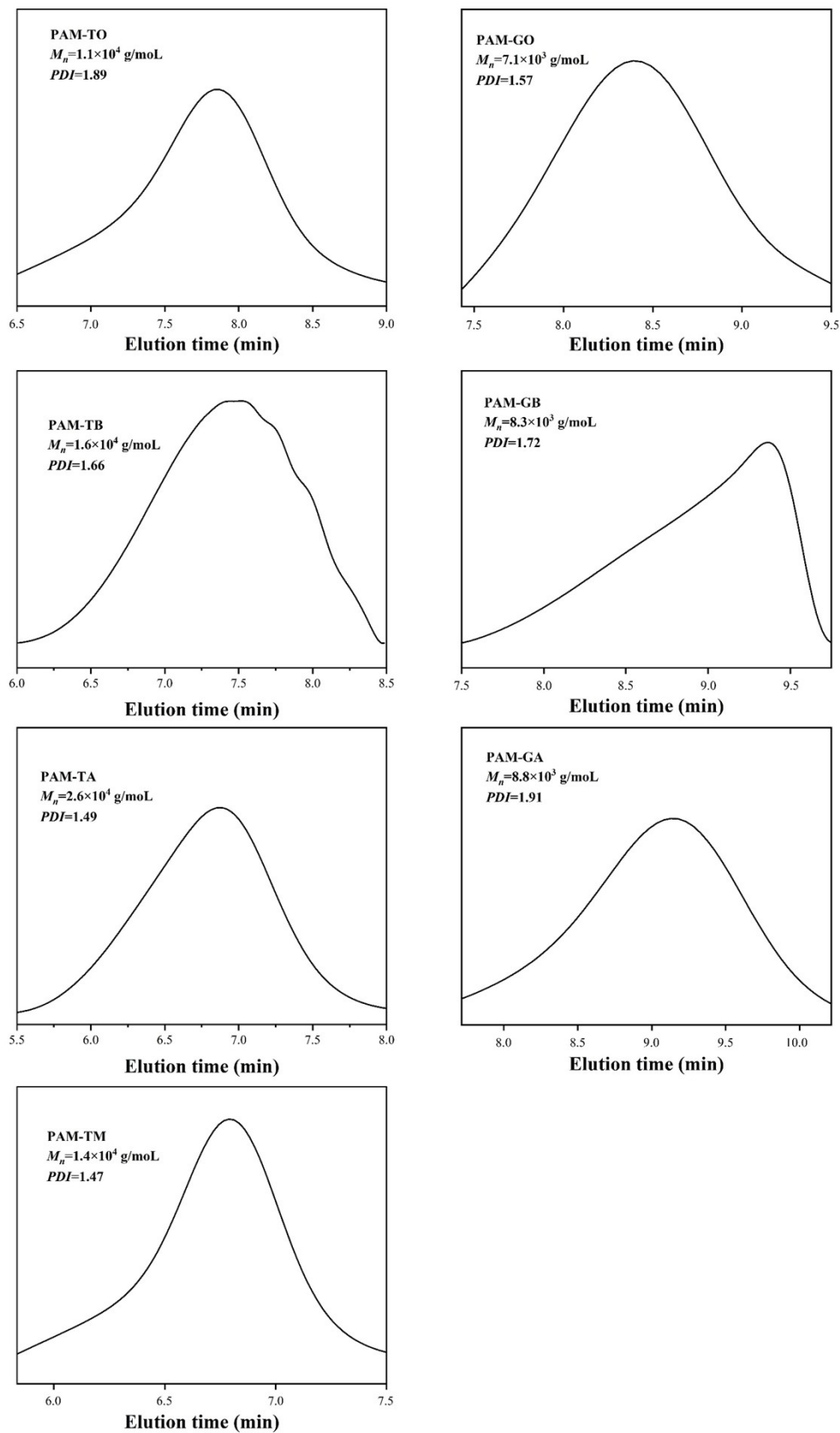


Fig. S3. GPC curves of PAMs.

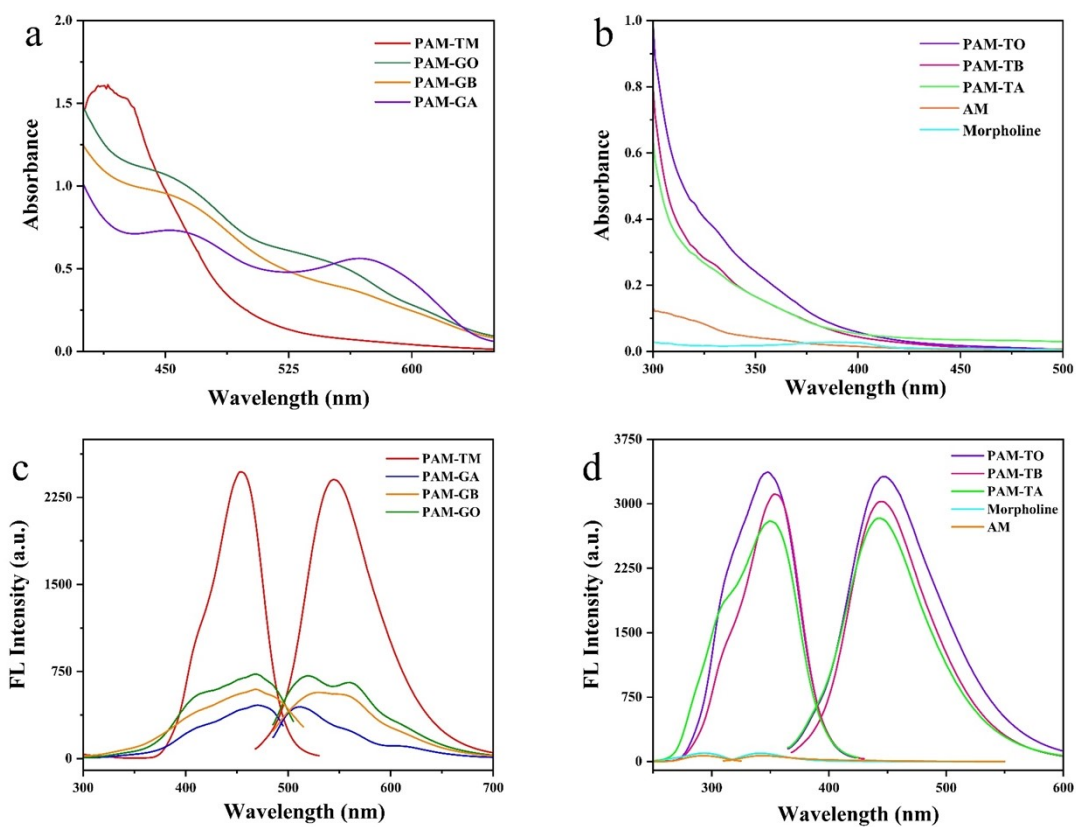


Fig. S4. UV and Fluorescence Spectra of PAMs and AM.

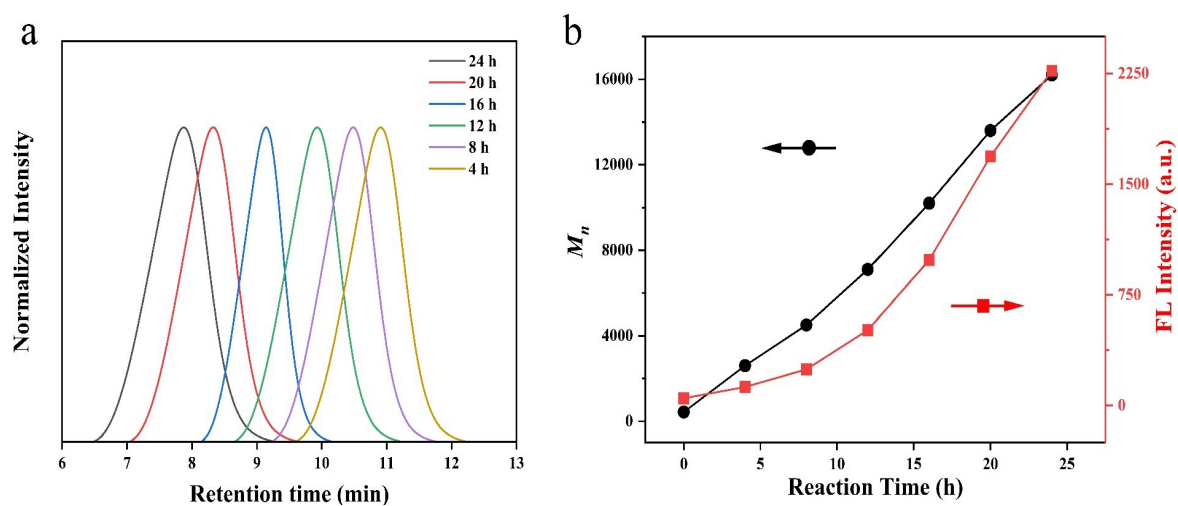


Fig. S5. M_n change of PAM-TB with polymerization time.

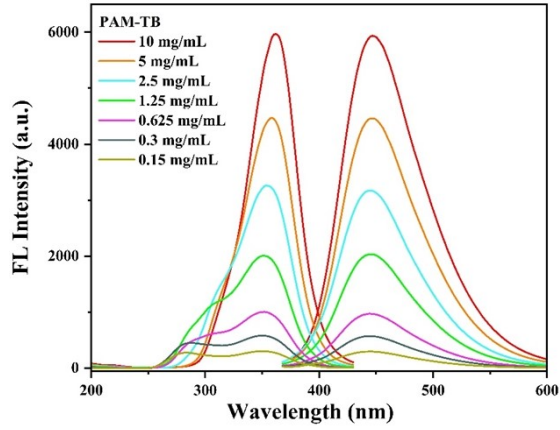


Fig. S6. Fluorescence spectra of PAM-TB solution with different concentration.

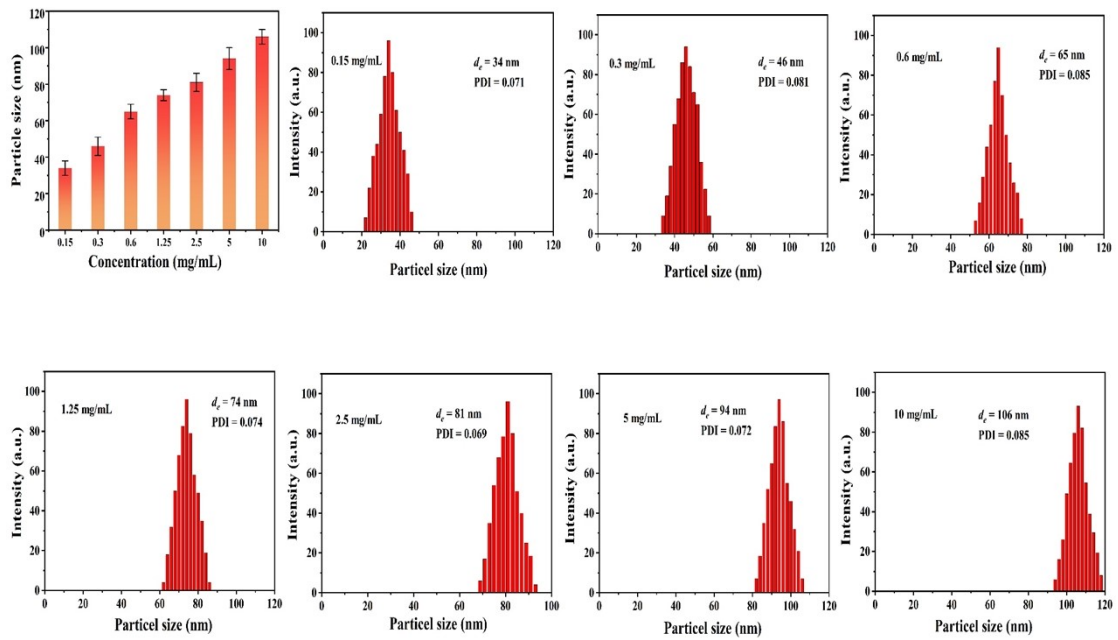


Fig. S7. Particle size plots of PAM-TB at different concentrations.

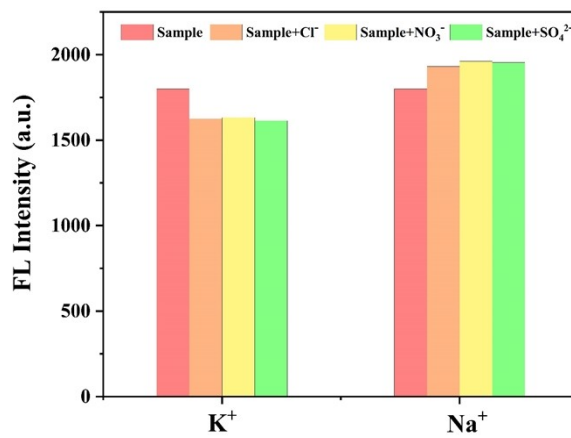


Fig. S8. The effect of anions on fluorescence intensity.

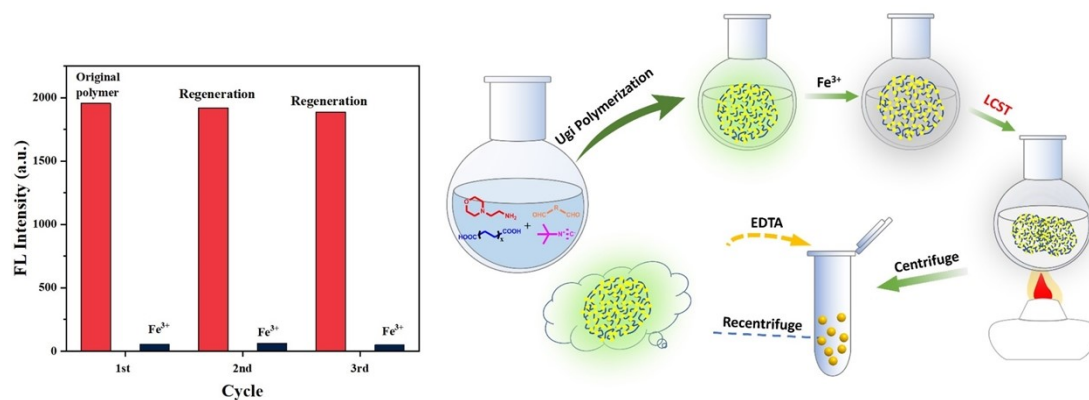


Fig. S9. Schematic illustration of PAMs reuse.

Preparation of test strips

We tried to test whether PAM-TB probe to Fe^{3+} ions could be applied in the solid state. By first immersing thin layer chromatography (TLC) plates in a PAM-TB solution, the PIE-active PAM-TB was uniformly adsorbed on the plates and displayed bright fluorescence under a portable 365 nm UV lamp, as shown Fig S10a. Then, the trace amounts of Fe^{3+} solution was spotted on the plate using a capillary, and the quenching of the fluorescence after the addition of Fe^{3+} ions was immediately seen under UV light. Actually, this quenching phenomenon can be clearly observed with the naked eye to identify the tested ions.

In addition, the filter paper was soaped in a solution of PAM-TB (5 mg/mL) in CHCl_2 to adsorb PAM-TB. After drying, the different concentrations of Fe^{3+} solutions were added dropwise to the treated filter paper, and we observed the paper surface under 365 nm UV light irradiation, the fluorescence change of the filter paper was clearly visible due to the quenching effect of Fe^{3+} . To determine the lowest visible detection concentration of Fe^{3+} ions by the fluorescence sensor, we dropped Fe^{3+} solutions with different concentrations onto the treated test paper. The filter paper was dried and observed fluorescence under UV light, as shown in Fig. S10b. The fluorescence intensity gradually decreased with the increase of Fe^{3+} ion concentration. It can be seen from the figure that when the Fe^{3+} ion concentration is 2 μM , the quenching effect of its fluorescence is negligible. Therefore, the PAM-TB-based test paper can be used as a portable sensitive fluorescence sensor with a minimum

detection concentration of 2 μM for Fe^{3+} ions. Moreover, we can restore the fluorescence of the test paper by introducing EDTA into the Fe^{3+} ion quenched test paper, thereby realizing the reuse of the fluorescent test paper, as shown in Fig. S10c.

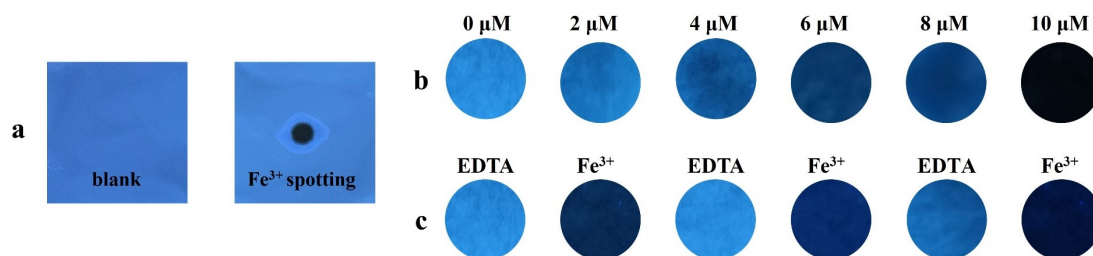


Figure S10. Visual test paper for Fe^{3+} ions

(a) Comparison of fluorescence photos before and after spotting Fe^{3+} solution on PAM-TB-deposited thin layer chromatography (TLC) plate; (b) Fluorescent test papers exposed to various concentrations of Fe^{3+} ; (c) Photographs of fluorescent test papers for Fe^{3+} detection and twice recycles after recovery by EDTA.

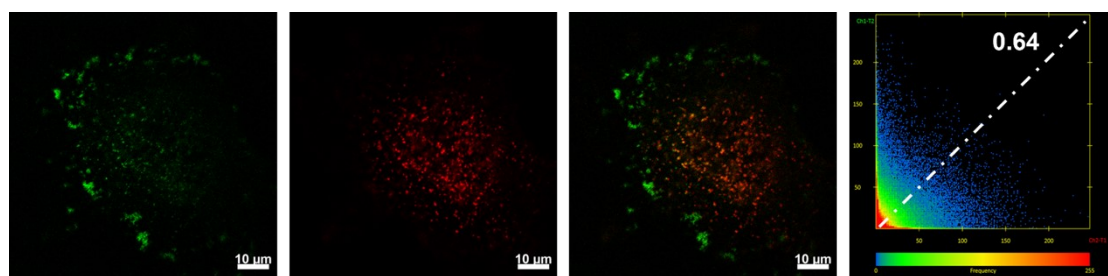


Fig. S11. Cell imaging experiments of PAM-TB

Confocal images of PC-12 cells stained with 1.0 μM PAM-TB and 50 nM LysoTracker Red: (A) Confocal image of PAM-TB on channel 1 ($\lambda_{\text{ex}} = 405 \text{ nm}$); (B) Confocal image of LysoTracker Red on channel 2 ($\lambda_{\text{ex}} = 633 \text{ nm}$); (C) Overlay of (B) and (D). Colocalization Coefficient of PAM-TM and LysoTracker Red. Scale bar =

10 μm

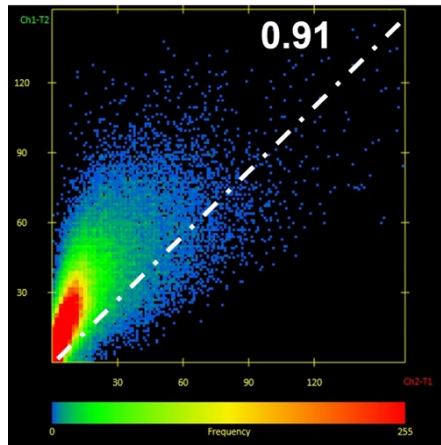


Fig. S12. Colocalization Coefficient of PAM-TM and LysoTracker Red in PC-12 cell.

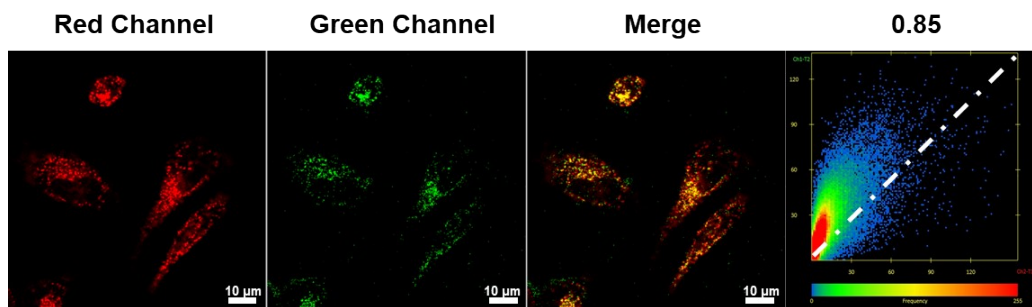


Fig. S13. Colocalization Coefficient of PAM-TM and LysoTracker Red in HeLa cell.

Confocal images of HeLa cells stained with 1.0 μM PAM-TM and 50 nM LysoTracker Red: (A) Confocal image of PAM-TM on channel 1 ($\lambda_{ex} = 488$ nm); (B) Confocal image of LysoTracker Red on channel 2 ($\lambda_{ex} = 633$ nm); (C) Overlay of (B) and (D). Colocalization Coefficient of PAM-TM and LysoTracker Red. Scale bar = 10 μm

Photobleaching resistance of PAM-TM in cells

(Left) F/F_0 (%) of fluorescent emission of PAM-TM (1.0 μM) and LysoTracker Red (50 nM) with increasing time. Green channel ($\lambda_{ex} = 488$ nm,); Red channel ($\lambda_{ex} = 633$ nm); (Right) fluorescent images of living PC-12 cells stained with PAM-TM (1.0 μM) and LysoTracker Red (50 nM) at 0 and 9 min. Scale bar = 10 μm

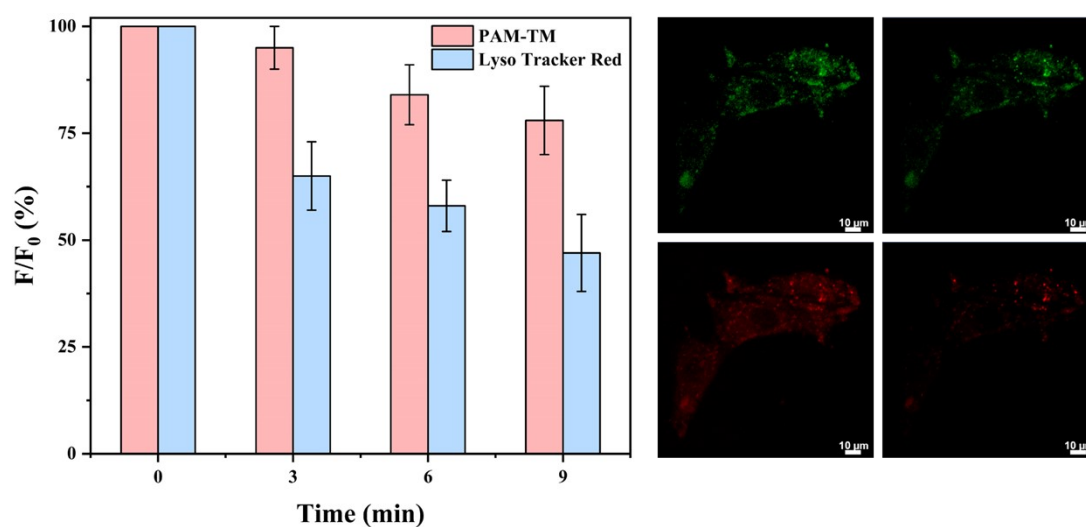


Fig. S14. Photobleaching resistance map of PAM-TM in cells.

Cytotoxicity assay

PC-12 cells in 96-well plates were rinsed with PBS and treated with DMEM supplemented with PAM-TM at the desired concentrations for 24 h. After that, the cytotoxicity of PAM-TM was examined by standard MTT assay according to the reported work.

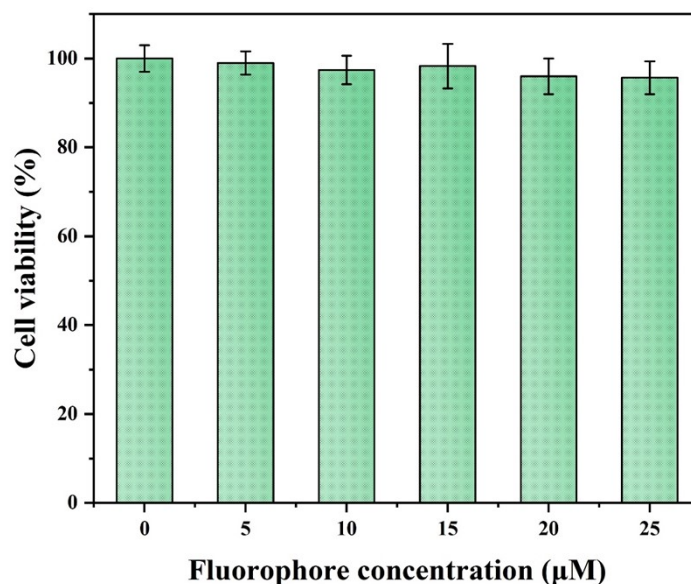


Fig. S15. Effects of PAM-TM on PC-12 cell viability.

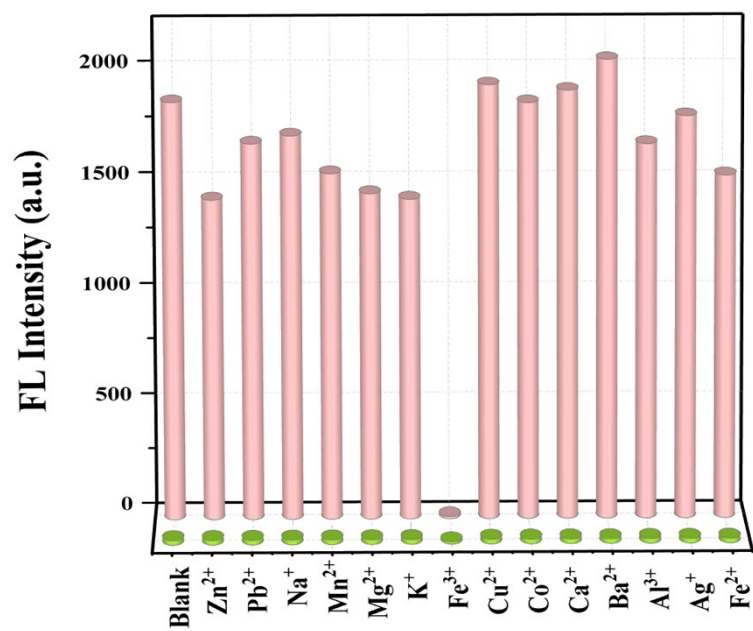


Fig. S16. Fluorescence intensity of PAM-TM in the presence or absence of interfering ions.

Table S3. A comparison between PAM-TM probes and the reported Fe³⁺-responsive fluorescent probes

REF	Targeting	Detection Limit (M)	Toxicity	Application
Zhang et al. (2020) ¹	no targeting studies	2.77×10 ⁻⁶	No toxicity studies	Hela Cell imaging
Huang et al. (2021) ²	no targeting studies	1.77×10 ⁻⁶	Low toxicity	Hela Cell/Zebrafish
Ye et al. (2019) ³	Lysosome	6.5×10 ⁻⁷	Low toxicity	C2C12 Cell imaging
Tumay et al. (2021) ⁴	no targeting studies	2.23×10 ⁻⁷	No toxicity studies	Water sample
Yu et al. (2021) ⁵	no targeting studies	1.4×10 ⁻⁸	low toxicity	Zebrafish in vivo imaging
Li et al. (2021) ⁶	no targeting studies	9.83×10 ⁻⁸	No toxicity studies	Hela Cell imaging
Geng et al. (2021) ⁷	no targeting studies	8.2×10 ⁻⁷	low toxicity	Hela Cell imaging
Xie et al. (2021) ⁸	no targeting studies	9.52×10 ⁻⁸	No toxicity studies	Water sample
Luo et al. (2016) ⁹	no targeting studies	1.24×10 ⁻⁸	No toxicity studies	PC-12 Cell imaging
Sing et al. (2019) ¹⁰	no targeting studies	1.32×10 ⁻⁶	No toxicity studies	Water sample
PAM-TM	Lysosome	5.4×10⁻⁸	low toxicity	PC-12 Cell imaging

References

1. Zhang, X.; Gou, Z.; Zuo, Y.; Lin, W., A novel polythioether-based rhodamine B fluorescent probe via successive click reaction and its application in iron ion detection and cell imaging. *Spectrochimica Acta Part A: Molecular and Biomolecular Spectroscopy* **2020**, *228*, 117679.
2. Huang, J.; Yan, Z.; Qiu, P.; Mo, Y.; Cao, Q.; Li, Q.; Huo, L.; Zhao, L., A New Coumarin-Acridone Compound as a Fluorescence Probe for Fe³⁺ and Its Application in Living Cells and Zebrafish. *Molecules* **2021**, *26* (8), 2115.
3. Ye, F.; Wu, N.; Li, P.; Liu, Y.-L.; Li, S.-J.; Fu, Y., A lysosome-targetable fluorescent probe for imaging trivalent cations Fe³⁺, Al³⁺ and Cr³⁺ in living cells. *Spectrochimica Acta Part A: Molecular and Biomolecular Spectroscopy* **2019**, *222*, 117242.
4. Tümay, S. O.; Irani-Nezhad, M. H.; Khataee, A., Multi-anthracene containing fluorescent probe for spectrofluorimetric iron determination in environmental water samples. *Spectrochimica Acta Part A: Molecular and Biomolecular Spectroscopy* **2021**, *248*, 119250.
5. Yu, L.; He, M.; Liu, S.; Dou, X.; Li, L.; Gu, N.; Li, B.; Liu, Z.; Wang, G.; Fan, J., Fluorescent Egg White-Based Carbon Dots as a High-Sensitivity Iron Chelator for the Therapy of Nonalcoholic Fatty Liver Disease by Iron Overload in Zebrafish. *ACS Applied Materials & Interfaces* **2021**, *13* (46), 54677-54689.
6. Li, B.; Gu, X.; Wang, M.; Liu, X.; Xu, K., A novel “off-on-off” fluorescent probe for sensing of Fe³⁺ and F⁻ successively in aqueous solution and its application in cells. *Dyes and Pigments* **2021**, *194*, 109637.
7. Geng, Y.; Chen, L.; Wan, Q.; Lian, C.; Han, Y.; Wang, Y.; Zhang, C.; Huang, L.; Zhao, H.; Sun, X.; He, H., A novel [1,2,4]triazolo[1,5-a]pyrimidine derivative as a fluorescence probe for specific detection of Fe³⁺ ions and application in cell imaging. *Analytica Chimica Acta* **2021**, *1187*, 339168.
8. Xie, B.; Lei, L.; Liu, E.; Bai, G.; Ye, R.; Xu, S., Blue-LED-excited Ce³⁺-doped alkaline-earth sulfide luminescent nanocrystals for selective and sensitive Fe³⁺ ions sensing. *Journal of Luminescence* **2021**, *230*, 117740.
9. Luo, A.; Wang, H.; Wang, Y.; Huang, Q.; Zhang, Q., A novel colorimetric and turn-on fluorescent chemosensor for iron(III) ion detection and its application to cellular imaging. *Spectrochimica Acta Part A: Molecular and Biomolecular Spectroscopy* **2016**, *168*, 37-44.
10. Singh, V. K.; M. Yadav, S.; Mishra, H.; Kumar, R.; Tiwari, R. S.; Pandey, A.; Srivastava, A., WS₂ Quantum Dot Graphene Nanocomposite Film for UV Photodetection. *ACS Applied Nano Materials* **2019**, *2* (6), 3934-3942.